Enhancing the Visible-Light Photoactivity of Silica-Supported TiO_2 for the Photocatalytic Treatment of Pharmaceuticals in Water

Carolina de Araújo Gusmão[1], Priscila Hasse Palharim[1], Bruno Ramos[1,2], Antonio Carlos Silva Costa Teixeira[1]

(1) Research Group in Advanced Oxidation Processes (AdOx), Department of Chemical Engineering, Escola Politécnica, University of São Paulo, Av. Prof. Luciano Gualberto, tr. 3, 380, São Paulo, SP, Brazil.

(2) Department of Metallurgical and Materials Engineering, Escola Politécnica, University of São Paulo, Av. Prof. Luciano Gualberto, tr. 3, 380, São Paulo, SP, Brazil.

carolina.argusmao@usp.br

Abstract

Catalyst samples based on SiO_2-supported TiO_2 were prepared with the incorporation of Ag (metal), S (non-metal), and ZnO@S (semiconductor and non-metal). The materials were evaluated regarding their morphological, optical, and crystalline properties as well as their photoactivity under visible and ultraviolet light towards the degradation rate of a model emerging pollutant, acetaminophen (ACT). All modified materials exhibited improved performance over the undoped catalyst. The Ag-doped catalyst achieved the largest degradation under visible radiation (about 30% in 120 min), whereas under ultraviolet irradiation, the ZnO@S-doped sample exhibited the best performance (about 62% in 120 min). A Doehlert design was carried out to evaluate the influence of pH and temperature on the photoactivity of Ag-TiO_2/SiO_2. In addition, the role of each reactive species in the photodegradation reaction was investigated by radical scavenger experiments, and the superoxide radical anion $O_2^{\bullet -}$ was shown to be the predominant reactive species. The stability of the Ag-TiO_2/SiO_2 material under ultraviolet and visible light was confirmed after five successive operation cycles, showing a reasonable (about 50%) loss of activity under visible irradiation, and a slight improvement (about 13%) under UV light, as a result of the photo-reduction of Ag^+. Lastly, the effect of the initial pollutant concentration showed that ACT

degradation using Ag-TiO_2/SiO_2 follows the Langmuir-Hinshelwood kinetics, with intrinsic reaction rate $k = 2.7 \times 10^{-7}$ mol L^{-1} under visible light radiation.

Keywords

TiO_2 photocatalysts, doped TiO_2 photocatalysts, visible light, pharmaceuticals, photodegradation.

1. Introduction

The use of pharmaceutically active compounds (PACs) in the maintenance of human and animal health is increasingly widespread (Kanakaraju et al. 2014). The annual average per capita consumption of these compounds in the world is estimated to be around 15 g, reaching up to 150 g in industrialized countries (Mohapatra et al. 2014). As a result, the presence of these compounds and their metabolites in aquatic environments has become an emerging environmental issue, particularly over the last 20 years. PACs are considered *contaminants of emerging concern* (CECs) due to the lack of proper regulation regarding their environmental disposal and the means for safeguarding it (especially in developing countries), and to their persistence in aquatic systems (Rivera-Utrilla et al. 2013; Kanakaraju et al. 2014). Some of the consequences brought about by these emerging pollutants are aquatic toxicity, the development of antigen-resistant bacteria, genotoxicity, and hormonal disruption (Ikehata et al. 2006; Rogowska et al. 2020; Taoufik et al. 2021). Furthermore, some mixtures of pharmaceutical compounds result in synergetic interactions, which are even more toxic to the aquatic environment. The presence of CECs in wastewaters, water bodies, and even drinking water clearly shows that conventional water treatment strategies are not sufficient to fully remove these contaminants (Taoufik et al. 2021).

Conventional water treatment systems usually consist of a series of physicochemical processes, followed by biological treatment. Physicochemical processes are inefficient to remove small, stable organic pollutant molecules, which are often difficult to metabolize by microorganisms present in biological slurries (Gadipelly et al. 2014). Instead, these compounds sometimes exhibit a negative effect, inhibiting the microorganisms or inducing bioaccumulation (Rivera-Utrilla et al. 2013). Thus, it is common to combine conventional systems with a more specific advanced efficient treatment. The most frequently applied combined techniques are adsorption, bioremediation, nanofiltration, and advanced oxidation processes (AOPs) (Kanakaraju et al. 2018; Akpotu et al. 2019). Most AOPs have attractive characteristics for the removal of emerging pollutants, such as robustness and high effectiveness. In

waters contaminated with pollutants of low solubility, AOPs are still considered the most cost-effective technology (Ikehata et al. 2006; Murgolo et al. 2021; Taoufik et al. 2021).

Heterogeneous photocatalysis mediated by a semiconductor, especially TiO_2, is currently one of the most widespread AOP technologies for drug removal studied in the literature. Titanium dioxide is the most widely used semiconductor in photocatalytic processes because of its high stability, non-toxicity, low cost, simple preparation and photoreactivity (Carp et al. 2004; Hashimoto et al. 2006; Ibrahim et al. 2020). The removal of aqueous CECs through heterogeneous photocatalysis occurs in four steps: (1) diffusion of molecules from the bulk solution to the TiO_2 surface; (2) adsorption of these molecules onto the surface; (3) photodegradation of molecules on the catalyst surface induced by light irradiation; and (4) desorption of the reaction products and release of these molecules back to the aqueous medium (Paumo et al. 2021).

Since the photooxidation reaction occurs on the TiO_2 surface, the extent of the catalytic surface area is highly determinant for the degradation efficiency. Therefore, in photocatalytic systems, TiO_2 is generally employed in nano size, whose surface-to-mass ratio is large. However, the cost of post-treatment separation of these nanoparticles from the treated effluent limits the application of these processes on a large scale, since the recovery of the catalyst requires intensive energy processes, raising the overall capital and operational costs (Alhaji et al. 2017; Ramos et al. 2021). A possible alternative to circumvent this disadvantage is to immobilize the catalyst on a support material, such as quartz, glass, zeolite, or silica gel, reducing or even eliminating downstream post treatment separation (Rincón and La Motta 2019). The use of silica gel as support for TiO_2 also brings other benefits: the Si−O−Si and Si−O−Ti bonds prevent the adhesion of anatase crystals, inhibiting their growth. In this way, the use of silica gel as a support can stabilize the crystalline phase of anatase, delaying its transformation to the rutile phase, therefore improving titanium dioxide photoactivity (Carp et al. 2004; Boyjoo et al. 2017).

On the other hand, titanium dioxide has drawbacks which limit its widespread application. Besides having poor activity in visible light due to its wide band gap (3.20 eV), its efficiency is impaired by the high charge recombination rate. A broad range of technologies have been investigated to overcome these limitations of TiO_2, such as modifying the semiconductor with metals, non-metals, and other semiconductors (Lim and Kim 2004; Zielińska-Jurek and Zaleska 2014). The use of metal ions modifies the TiO_2 electronic structure by introducing new energy levels in the band gap, enabling photons with lower energy to be excited from the valence band to the conduction band (Paumo et al. 2021), enhancing

the visible light responsiveness of TiO_2. Additionally, metal nanoparticles, such as Ag, whose Fermi energy is lower than the conduction band of semiconductors, trap photogenerated electrons, improving charge separation, which also enhances TiO_2 photocatalytic activity (Carp et al. 2004; Chen et al. 2020). For non-metal doping, oxygen is replaced by anions, such as S^{2-} and N^{3-}, which promote band gap narrowing, improving photocatalytic activity under visible light (Carp et al. 2004; Chen et al. 2020; Paumo et al. 2021). Despite improving the visible-light photocatalytic activity of TiO_2, single doping usually has no significant effect when visible-light and UV photoreactivity are compared. Several studies have explored co-doping as a potential approach to overcome this issue. However, co-doping may not necessarily enhance TiO_2 photoactivity (Kim et al. 2014), which highlights the importance of comparing different dopants and formulations in order to assess which doping is most appropriate for narrowing the band gap energy of TiO_2 and reducing charge recombination, in the photocatalytic degradation of emerging pollutants.

To the best of our knowledge, there are no previous studies dedicated to the synthesis of TiO_2 supported on silica gel together with its doping with different materials aiming to compare its properties and activities in the photocatalytic degradation of pharmaceutical compounds. Given the mentioned context, the purpose of the current study is to carry out an unprecedented screening, synthesizing metal (Ag-doped), non-metal (S-doped), and co-doped (ZnO@S-doped) photocatalysts supported on silica gel, and comparing their activities in pharmaceutical photodegradation, using acetaminophen (ACT) as a model contaminant. Subsequently, an extensive investigation was carried out in the assessment of the reaction operational parameters, photodegradation mechanisms and stability of the catalyst photoactivity.

2. Materials and Methods

2.1. Materials

Titanium isopropoxide, TTIP ($Ti[OCH(CH_3)_2]_4$, ACS, ≥ 97%), silica gel 63-200 μm, acetaminophen (HPLC, ≥ 99%), silver nitrate ($AgNO_3$ ACS, PA), thioureia (NH_2CSNH_2, ACS ≥ 99%), zinc acetate ($(CH3CO_2)_2Zn$ ACS, ≥ 99%) and zinc nitrate ($Zn(NO_3)_2{\cdot}6H_2O$ ACS, ≥ 99%) were purchased from Sigma-Aldrich. Diluted nitric acid (1.0 mol L^{-1} HNO_3), ammonium hydroxide (1.0 mol L^{-1} NH_4OH), sodium hydroxide (1.0 mol L^{-1} NaOH), isopropanol, ethanol and Milli-Q® water were of analytical grade.

2.2. Synthesis of pure TiO_2/SiO_2

The coating of silica gel (SiO_2, 300 m^2 g^{-1} specific surface area) with TiO_2 crystals was conducted using the acid sol-gel method described by Chen et al. (2004). A TiO_2 precursor solution was prepared by slowly dripping 8.4 mL of TTIP into a 1-mol L^{-1} HNO_3 solution under vigorous stirring. After 60 min, 60 mL of Milli-Q® water and a 1.0-mol L^{-1} NaOH solution were added until the pH reached 2.0. After 1 hour of vigorous stirring, 9.0 g of silica gel were added and the pH was raised to 3.0 through the addition of a 1.0-mol L^{-1} NaOH solution. The gel formed was then washed, dried at 80 °C and calcined at 450 °C.

2.3. Synthesis of doped TiO_2/SiO_2

Synthesis of Ag-TiO_2/SiO_2. The synthesis of silver-doped TiO_2/SiO_2 was adapted from Chen et al. (2004) and Choi et al. (1994). Firstly, a TiO_2 precursor solution was prepared by slowly adding 8.4 mL of TTIP into a 1.0-mol L^{-1} HNO_3 solution. After 60 min, the solution pH was increased to 1.5 by adding 1.0-mol L^{-1} NaOH, and 0.08 g of $AgNO_3$ was also added. Subsequently, the pH was raised to 2.0, and 9.0 g of silica gel was added. Finally, the pH was increased to 3.0 and the gel was washed, dried at 80 °C and calcined at 450 °C.

Synthesis of S-TiO_2/SiO_2. The synthesis of sulfur-doped TiO_2/SiO_2 was adapted from Chen et al. (2004) and Ohno et al. (2004). First, 8.4 mL of TTIP and 8.6 g of thiourea were mixed in absolute ethanol under vigorous stirring. 60 min later, the pH was decreased to 1.5 by adding 1.0-mol L^{-1} HNO_3 solution. After the sol was formed, the pH of the solution was increased to 2.0 by adding 2.0-mol L^{-1} NaOH, and 9.0 g of silica gel was also added. Finally, the pH was increased to 3.0 and subsequently the gel was washed, dried at 80 °C and calcined at 450 °C.

Synthesis of S@ZnO-TiO_2/SiO_2. The synthesis of ZnO@S-doped TiO_2/SiO_2 was adapted from Chen et al. (2004) and Chu et al. (2017). Initially, 8.4 mL of TTIP was mixed with absolute ethanol. Simultaneously, a deionized water solution containing 1.18 g of thiourea and 0.53 g of zinc acetate was prepared. Subsequently, the solutions were mixed. After 60 min of vigorous stirring, 5.2 mL of 1.0-mol L^{-1} HNO_3 solution was added for gel formation. One hour later, the pH was increased to 2.0 by adding 1.0-mol L^{-1} NaOH solution, and 9.0 g of silica gel were added. Finally, the pH was increased to 3.0 and subsequently the gel was washed, dried at 80 °C and calcined at 450 °C.

2.4. Analyses and experimental investigations

Characterization. The morphology and particle size of the catalysts were investigated in a Quanta 650 FEG (Bruker) scanning electron microscope (SEM). X-ray photoelectron spectroscopy (EDS) analyses were carried out in a microanalysis system (Quantax, Bruker) equipped with a silicon drift detector (SDD) to gather semi-quantitative information about the composition of the catalyst surface. Crystalline phases and crystal sizes of TiO_2, were evaluated by X-ray diffraction in the range 2θ = 10-80° at a scan rate of 0.02° s^{-1} in a X'Pert Diffractometer (Phillips) using Cu-Kα (0.154 nm) radiation and a tube power of 1.6 kW (40 kV at 40 mA). For crystal size determination, the Scherrer equation ($D = 0.\lambda/\beta\cos\theta$) was used, where D is the average crystal size; B is the width of the diffraction peak at half maximum height; λ is the wavelength of the electromagnetic radiation used in the equipment and θ is the Bragg angle of diffraction. The optical properties of the catalyst were evaluated by diffuse reflectance spectroscopy (DRS) using a UV 2550 (Shimadzu) equipment.

Photocatalytic activity. The photocatalytic activity tests were performed in a batch reactor, consisting of a jacketed 50-mL beaker connected to a thermostatic water bath for temperature control, as shown in Fig. 1a. Acetaminophen (ACT) was selected as the model emerging pollutant for comparison of photocatalytic activities. In each experiment, 100 mg of catalyst was dispersed in 50 mL of a 5.0-mg L^{-1} aqueous ACT solution, prepared in deionized water. Initially, the suspension was stirred for 30 min in the dark to reach adsorption-desorption equilibrium. Subsequently, the reactor was irradiated by four LEDs chips (Lartec 100W, with maximum emission at 430 nm), or by one UV-A LED chip (LG 50W, with maximum wavelength at 365 nm), depending on the operational conditions of the experiment (under conditions of ultraviolet or visible light irradiation). The irradiation source was positioned perpendicularly 15 cm away from the solution surface. The irradiance spectra of the light sources at this distance are shown in Fig. 1b. The integrated irradiance (31.0 mW cm^{-2} and 3.4 mW cm^{-2} for visible and UV-A LED chips, respectively) was measured by a spectroradiometer (Luzchem, SPR-4002). 1.0-mL samples were collected over time and filtered through 0.45-μm PVDF membranes to remove the catalyst particles. Residual acetaminophen in the samples was quantified by UPLC (Shimadzu LC20) using UV-VIS detection (SPD20A) after separation in a C18 column (Prominent). The mobile phase consisted of methanol and water (25:75 v/v), at a flow rate of 1.0 mL min^{-1}; the injection volume and the oven temperature were set at 50 μL and 35 °C, respectively. The detection wavelength was 243 nm and the retention time was approximately 7 min. The first batch of experiments was performed to evaluate the photocatalytic activities of TiO_2/SiO_2 samples doped with different materials under visible or ultraviolet light irradiation for 120 min. For these

runs, the initial pH of the working solution was around 6 (with no adjustment) and the solution temperature was 30 °C.

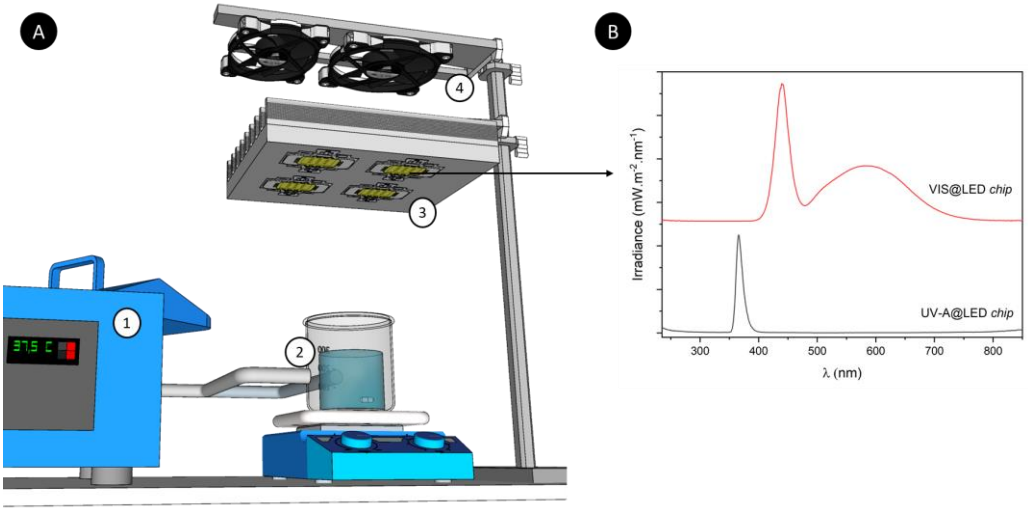

Fig. 1 a) Description of the experimental unit: 1. Thermostatic water bath; 2. Jacketed beaker; 3. LED chips coupled to a heatsink; 4. Fan cooling system; b) Irradiance spectra of UV-A and visible light irradiation sources

2.5. Doehlert experimental design

A Doehlert experimental design (Doehlert 1970) was applied to investigate the optimum operating conditions for ACT degradation using the photocatalyst that showed the best photocatalytic performance during the first batch of experiments. A Doehlert matrix with two variables was built, for the initial pH of the working solution (X_1) and the reaction temperature (X_2). These two variables and their levels were chosen to represent parameters that could potentially exert significant effect on the photocatalytic activity. A total of nine runs were performed, with three replicates at the central point conditions for statistical validation, according to Table 1.

Table 1 Doehlert experimental design to evaluate the effects of pH and temperature on the photocatalytic activity for acetaminophen (ACT) degradation

Schematic illustration	Run	Coded levels		Real variables		Response		
		X_1	X_2	pH_0	Temperature (°C)	ACT degradation[a] (%)	k^a ($\times 10^{-3}$ min^{-1})	R^2
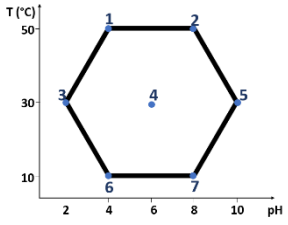	1	–0.5	0.866	4	50	41.0	4.40	0.990
	2	0.5	0.866	8	50	44.5	4.77	0.991
	3	–1	0	2	30	15.0	1.45	0.970
	4	0	0	6	30	31.9	3.31	0.989
	4[a]	0	0	6	30	30.7	2.94	0.995
	4b	0	0	6	30	31.6	3.37	0.983
	5	1	0	10	30	39.5	4.43	0.984
	6	–0.5	–0.866	4	10	31.5	3.45	0.971
	7	0.5	–0.866	8	10	34.1	3.85	0.959

[a] Calculated for 120 min of reaction.

2.6. Radical scavenging experiments

Finally, a series of experiments with radical scavengers was carried out to verify the main oxidation mechanism in the process adopting the catalyst with the best photocatalytic performance during the first batch of experiments. The initial pH and temperature of the working solution reproduced the central point of the Doehlert experimental design (pH_0 = 6; T = 30 °C). A dose of 100 mg of catalyst was dispersed in 50 mL of a 5.0-mg L^{-1} ACT solution, previously adjusted to the target pH. Then, the scavenger agents, shown in Table 4, were added to the reaction and the experiments were performed as described in section 2.4.

3. Results and discussion

3.1. Photocatalyst characterization

3.1.1. Scanning Electron Microscopy and EDS

The morphology of ZnO@S-TiO_2/SiO_2, S-TiO_2/SiO_2 and Ag-TiO_2/SiO_2 samples obtained by SEM analysis are shown in Fig. 2A, B and C, respectively. The silica particles have irregular shapes and

equivalent diameter (D_{eq}) ranging from 80 to 120 μm. Some clusters, marked by white circles, can also be observed. They consist of doped TiO_2 crystals not supported on the SiO_2 particles, as can be confirmed by the EDS spectra of points on these clusters. Despite the presence of these TiO_2 agglomerates, some authors suggest that the use of silica gel as support reduces the clusters amount, preventing their formation (Mazabuel-Collazos and Rodríguez-Páez 2018a; Zhou et al. 2020). This may be connected to the favorable formation of Si−O−Ti over Ti−O−Ti bonds in the synthesis procedure (described in Section 2.2, through pH adjustment (Bischoff and Anderson 1995).

Fig. 2D, E and F present EDS spectra of Ag-, S- and ZnO@S-doped TiO_2/SiO_2 samples, at points on both doped TiO_2 clusters and SiO_2-supported doped-TiO_2. These points are indicated and related to the corresponding spectra by numbers 1, 2, 3, 4, 5 and 6, as shown in Fig. 2. These spectra confirm the success of the doping procedure. However, due to the low ZnO and S contents employed in the synthesis method, peaks referring to zinc and sulfur were hardly detected in the spectrum shown in Fig. 2F. The variations in the relative Ti and Si peaks of the different samples are attributed to the different angulations and samplings of the measured EDS spectra (Dey et al. 2020).

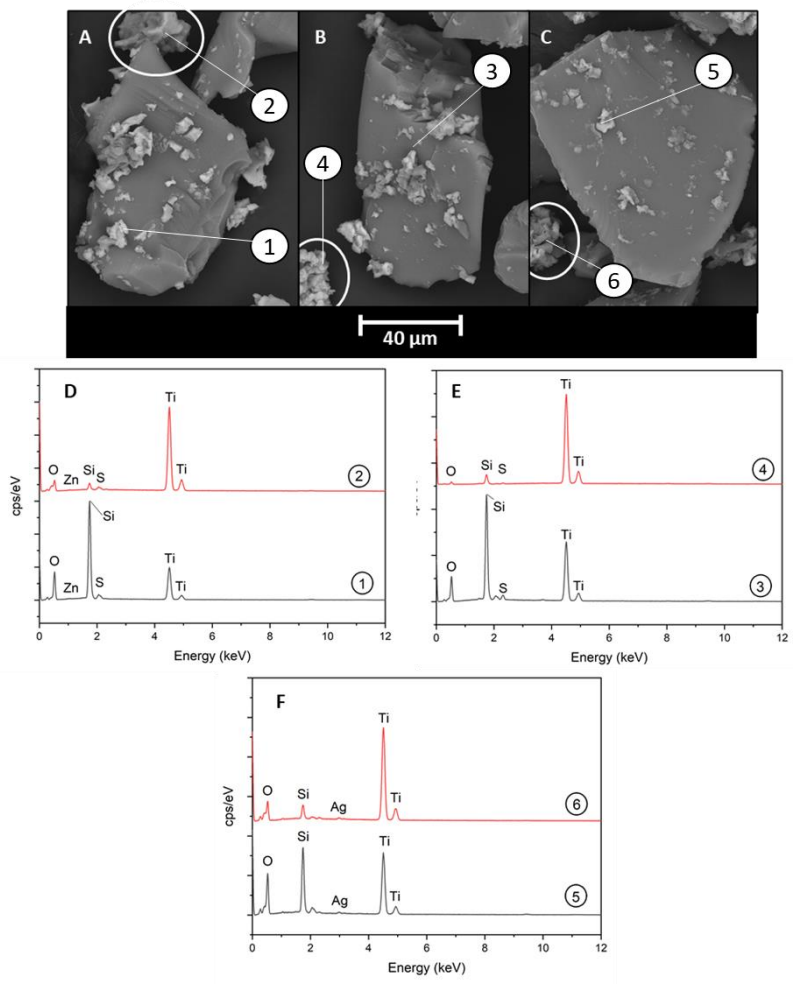

Fig. 2 SEM images of samples: a) ZnO@S-TiO_2/SiO_2; b) S-TiO_2/SiO_2; c) Ag-TiO_2/SiO_2; EDS spectra of samples: d) ZnO@S-TiO_2/SiO_2; e) S-TiO_2/SiO_2; f) Ag-TiO_2/SiO_2

3.1.2. UV-VIS Spectroscopy

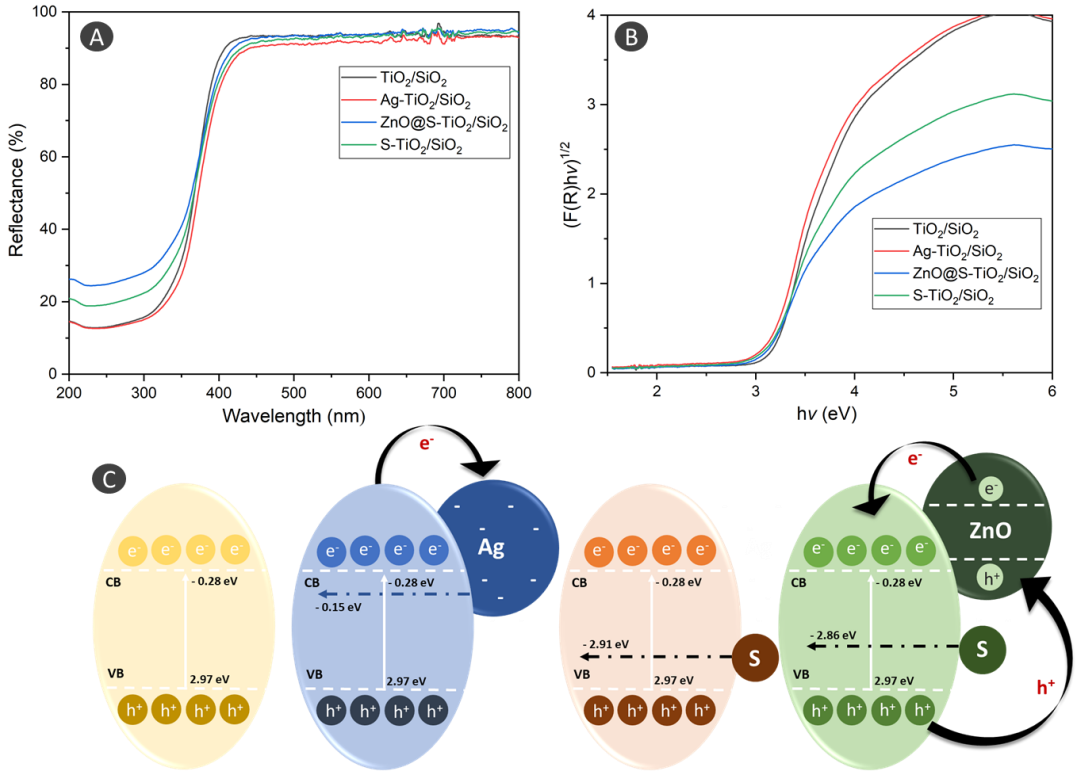

Fig. 3 a) UV-VIS reflectance spectra of pure and doped TiO_2/SiO_2 catalysts; b) Kubelka-Munk function of the synthesized samples; c) Schematic process of charge transfer in pure and doped TiO_2/SiO_2 catalysts

Fig. 3a shows the diffuse reflectance spectra of the different catalysts. It is clear that the doping of TiO_2/SiO_2 with Ag, S and ZnO@S increased the UV-VIS light absorption and extended the absorption edge into the visible region. As an enhancement in light absorption leads to an increase in electron-hole pair generation, this may improve the photocatalytic activity of TiO_2 under visible-light irradiation. With regard to Ag-TiO_2/SiO_2, it is proposed that Ag clusters on the TiO_2 surface act as scattering centers, resulting in surface plasmon resonance, which increases light absorption (Dey et al. 2020). Furthermore, the extension of light absorption into the visible region is correlated with the generation of new energy states introduced by the Ag nanoparticles. These nanoparticles also act as electron traps, increasing charge separation and reducing their recombination rate (Carp et al. 2004; Xu et al. 2017; Dey et al. 2020; Zhang et al. 2021).

The band gap energies were obtained through the Kubelka-Munk model, calculating the function F(hν), as a function of the hν energy and reflectance (R), (Mazabuel-Collazos and Rodríguez-Páez 2018). This function is calculated from Eq. 1, and the band gap energy is estimated by extrapolating the absorption edge to its intersection with the horizontal axis.

$$F(hv) = \left(\frac{(1-R)^2}{2R}\right)^{0.5} \quad (1)$$

We found from Fig. 3b and Table 2 that the band gap energy of the doped catalysts was lower than that of the undoped TiO_2/SiO_2 sample. The UV-VIS spectrum of S-TiO_2/SiO_2 also showed an extension of light absorption into the visible region. This is consistent with the results reported in the literature (Wei et al. 2008; Niu et al. 2012; Chen et al. 2019). We hypothesize that the band gap narrowing is a consequence of the replacement of TiO_2 lattice oxygen by sulfur (Carp et al. 2004). This introduces new electronic levels in the structure and enables a greater generation of electron-hole charge pairs at lower wavelength energies, i.e., in the visible light region (Niu et al. 2012). It is also noticeable from Fig. 3a that the diffuse reflectance spectrum of ZnO@S-TiO_2/SiO_2 showed a slight absorption spread in the visible light region. This is favored by the synergistic effect of TiO_2 and ZnO semiconductors, associated with S-doping (Zhou et al. 2020). The coupling of semiconductors with distinct conduction and valence bands favors charge separation, increases the lifetime of the charge carriers and improves the interfacial charge transfer with the reagents adsorbed on the photocatalytic surface (Carp et al. 2004; Chu et al. 2017; Mazabuel-Collazos and Rodríguez-Páez 2018a). The ZnO@S doping of TiO_2 leads to electronic transitions involving new energy states generated by surface defects (Fig. 3c). With regard to ZnO, charge transfer between O^{2-} from TiO_2 and Zn^{2+} may occur induced by the electron excitation from the valence band (consisting of oxygen 2p orbitals) to the conduction band (formed by zinc 3d orbitals) (Mazabuel-Collazos and Rodríguez-Páez 2018b).

3.1.3. X-ray Diffractometry

The XRD patterns of the synthesized samples showed peaks at 2θ = 24.12º, 37.5º, 48.2º and 54.4º, referring to the crystal planes (101), (004), (200), (105) and (204) of the TiO_2 anatase phase (Zhou et al. 2020). Due to the use of silica gel as support, the poor crystalline nature of the materials is present in all diffractograms. The peak located at 2θ = 24.1º, referring to the plane (101), is slightly shifted to 2θ = 25.2º in the doped samples, evidencing the presence of dopants in the crystalline structure of TiO_2 anatase (Dey et al. 2020). No peaks referring to ZnO were observed in ZnO@S-TiO_2/SiO_2 due to the low content of the metal oxide in the material (Tobajas et al. 2017). The crystallite sizes as well as lattice parameters are shown in Table 2 and were calculated from the XRD patterns. It is observed that the doped materials have lower crystallite sizes than the undoped TiO_2@SiO_2. This serves as evidence that doping with Ag, S and ZnO@S inhibited crystal growth through the formation of Ti−O−Ag, Ti−O−S and Ti−O−Zn bonds,

respectively, which prevent grain nucleation (Chen et al. 2019; Dey et al. 2020; Nguyen et al. 2020; Zhang et al. 2021). This reduction in crystal size can be extremely favorable to photocatalytic activity, since it favors the separation of photogenerated charges (Carp et al. 2004).

Table 2 Synthesis conditions and characterization results of the photocatalytic materials

Material	Dopant	Precursor	Content (%)	Lattice parameters (Å)		Microstrain (ε)	Crystal size (nm)	Band gap (eV)
				a = b	c			
TiO_2/SiO_2	–	–	–	3.78	9.31	0.011	4.28	3.26
Ag-TiO_2/SiO_2	Ag	Silver Nitrate	0.3	3.76	9.35	0.014	3.42	3.13
S-TiO_2/SiO_2	S	Thiourea	1.3	3.52	10.35	0.096	4.18	3.20
ZnO@S-TiO_2/SiO_2	ZnO@S	Zinc nitrate/thiourea	1% S/ 0.1% ZnO	3.78	9.43	0.012	3.83	3.15

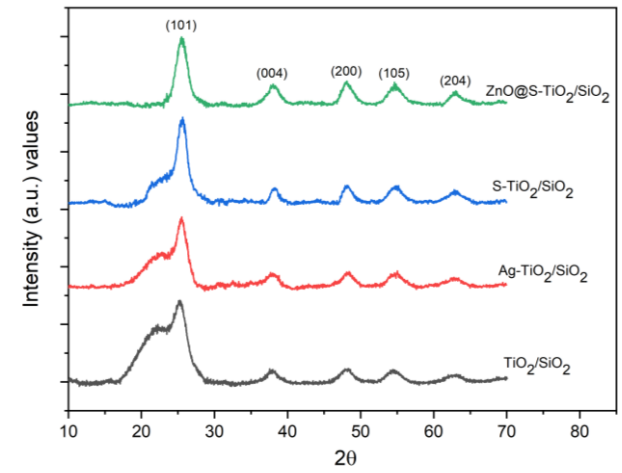

Fig. 4 XRD patterns of TiO_2/SiO_2, Ag-TiO_2/SiO_2, S-TiO_2/SiO_2 and ZnO@S-TiO_2/SiO_2

Moreover, it is observed in Table 2 that the unit cell parameters changed significantly in the doped samples, especially in S-TiO_2/SiO_2 and ZnO@S-TiO_2/SiO_2. This evidences that these dopants are present in the TiO_2 crystalline lattice, affecting the internuclear forces due to the unbalanced charges generated (Wei et al. 2008; Dey et al. 2020). Although the changes in the lattice parameters are small for the Ag-TiO_2/SiO_2 catalysts, the results are within the order of magnitude or even higher than those found in the literature (Dey et al. 2020; Aini et al. 2019). For example, Dey et al. (2020) found even smaller variations in lattice parameters comparing (1% Ag)-TiO_2 with pure TiO_2, while Aini et al. (2019) found no

significant alterations comparing pure titanium dioxide and TiO_2 catalysts containing 1% Ag. As we worked with a lower content of 0.3%-Ag, the modifications of the lattice parameters found in our work would suffice to indicate the Ag-doped effect on the TiO_2 lattice distortion. Table 2 also shows an increase in microstrain in doped samples, compared to the undoped TiO_2. This was expected, due to the replacement of O^{2-} by sulfur ions, whose ionic radii are different, leading to crystal distortion (Wei et al. 2008).

3.2. Performance of different doped catalysts under visible and UV radiation

The prepared catalysts were evaluated for their photoactivity to acetaminophen (ACT) degradation in aqueous medium under visible and UV irradiation. Table 3 and Fig. 5 summarize the main results of this investigation. Control runs performed in the absence of SiO_2-supported TiO_2 catalysts confirmed that no appreciable photolysis of acetaminophen occurred after 180 min of irradiation using the same LEDs light sources. This result is consistent with the very low ACT absorption above 300 nm (Martignac et al. 2013). The Ag-doped catalyst exhibited the best photocatalytic activity under visible light, achieving 38.2% ACT degradation. This material showed the most pronounced reduction in band gap energy when compared to the undoped catalyst. Its improved activity under visible light may be associated with the generation of new energy states close to the conduction band, introduced by Ag nanoparticles, allowing the generation of electron-hole pairs through absorption of less energetic photons. Among the doped catalysts, ZnO@S-TiO_2/SiO_2 exhibited the smallest extent of ACT degradation (10.5%) (Table 3 and Fig. 5a), which is probably due to the low content of dopants in the TiO_2 crystalline structure, as indicated by EDS and XRD analyses.

Table 3 Photoactivity of the pure and doped catalysts under UV and visible irradiation

Type of irradiation	VIS		UV-A	
Response / Sample	Degradation	Rate constant (min^{-1})	Degradation	Rate constant (min^{-1})
Photolysis	0.06 µmol ACT/g cat. (0.33%)	2.7×10^{-5}	0.19 µmol ACT/g cat. (1.11%)	9.3×10^{-5}
TiO_2/SiO_2	0.17 µmol ACT/g cat. (1.0%)	8.1×10^{-5}	5.3 µmol ACT/g cat. (33.7%)	3.5×10^{-3}
Ag-TiO_2/SiO_2	6.3 µmol ACT/g cat. (38.2%)	4.0×10^{-3}	7.9 µmol ACT/g cat. (46.0%)	5.1×10^{-3}

$S\text{-}TiO_2/SiO_2$	4.5 µmol ACT/g cat. (28.2%)	2.7×10^{-3}	5.3 µmol ACT/g cat. (34.6%)	3.6×10^{-3}
$ZnO@S\text{-}TiO_2/SiO_2$	1.7 µmol ACT/g cat. (10.5%)	9.7×10^{-4}	10.6 µmol ACT/g cat. (61.7%)	8.1×10^{-3}

The undoped catalyst did not show any appreciable activity under visible light (Fig. 5A), which was expected due to its wider band gap energy, corresponding to an absorption edge into the UV region. The S-doped catalyst showed a slightly lower ACT degradation rate than the Ag-doped material (28.2%). As mentioned in Section 3.1.2, this behavior is associated with the narrowing of the band gap energy promoted by the introduction of intermediate energy levels by sulfur.

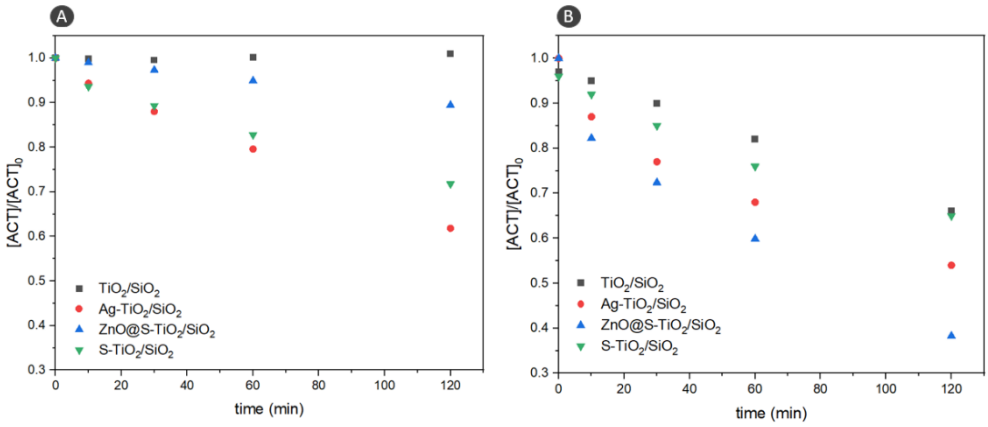

Fig. 5 Photocatalytic performance of TiO_2/SiO_2-based photocatalysts in the degradation of acetaminophen ($[ACT]_0 = 4.93 \pm 0.08$ mg L^{-1}) under: a) Visible radiation; b) UV-A radiation

From Table 3, we observe that the photocatalytic activities of the materials under UV-A and visible radiation follow different patterns.. The sample $ZnO@S\text{-}TiO_2/SiO_2$, which showed the lowest photoactivity under visible light, was the one that showed the best activity under UV-A (61.7%) (Fig. 5b). The presence of ZnO in the structure of TiO_2, although in small quantities, favors the separation of e^-/h^+ charges and increases their lifetime, leading to an improvement in the catalyst performance. The Ag-doped photocatalyst also showed superior photoactivity under UV-A light when compared to the undoped sample, reaching 46.0% degradation. However, we note that the increase was not as significant compared to the ZnO@S-doped TiO_2. The Ag nanoparticles present in the material act as electron traps, as illustrated in Fig. 3b, favoring charge separation and improving the overall photoactivity. On the other

hand, the S-doped catalyst showed ACT degradation almost equal to that of the undoped catalyst. This performance can be attributed to the fact that in this case doping did not improve charge separation, but simply extended the absorption band into the visible-light region.

3.3. Evaluation of catalyst stability under reuse cycles

The catalyst Ag-TiO_2/SiO_2 was chosen for stability evaluation along successive cycles of reuse under visible and UV-A radiation due to its good activity in the photocatalytic degradation of acetaminophen under visible light, combined with its lower band gap energy. From Fig. 6a, we observe that the Ag-TiO_2/SiO_2 catalyst considerably decreased its activity under visible light throughout five reaction cycles, while under UV light the activity increased. Fig. 6b shows that after the cycles under visible radiation, there was a significant detachment of the supported TiO_2 nanocrystals out of the silica particles. In contrast, we observe that the catalyst after reuse under UV radiation showed reduction in particle size, and the formation of pure TiO_2 agglomerates.

Fig. 6b shows a visible growth in Ag peaks in the EDS analysis of the catalyst after UV reuse, when compared to the fresh catalyst. We assume that the surface-segregated Ag^+ ions were photo-reduced by UV irradiation to Ag^0, increasing the content of metallic silver on the catalyst surface, and intensifying the effect of the dopant in the photocatalytic activity (Zhang et al. 2021). The drop in the activity of the catalyst under visible irradiation is likely related to the silica gel particles with considerably fewer supported TiO_2 crystals after VIS reuse, as shown in SEM images (Fig. 6). The leached titanium dioxide agglomerated, reducing the irradiated area, as a part of the TiO_2 crystals were covered by other crystals in the TiO_2 clusters, which hinders them from absorbing light. The effect of the decreased irradiated area by TiO_2 agglomerates is not observed in the catalyst after UV light reuse due to the higher Ag content acting as scattering centers, increasing light absorption, as mentioned in Section 3.1.2.

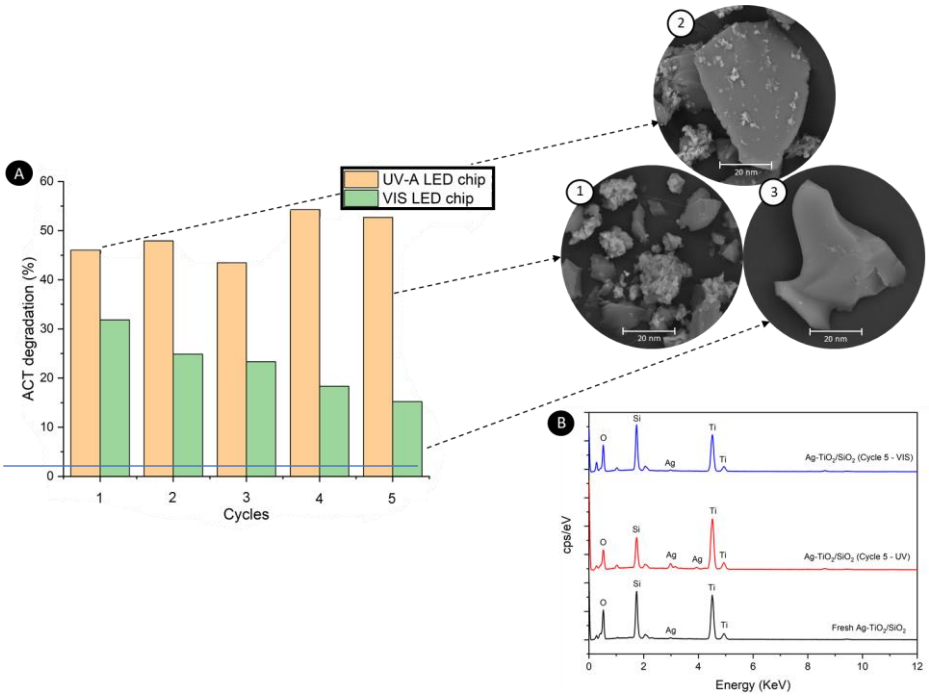

Fig. 6 a) ACT degradation for fresh, UV and VIS reused Ag-TiO_2/SiO_2 catalysts, and morphology for UV reused Ag-TiO_2/SiO_2 (1), fresh (2) and VIS reused Ag-TiO_2/SiO_2 (3); b) EDS spectra for fresh, UV and VIS reused Ag-TiO_2/SiO_2

3.4. Influence of pH and temperature on the photoactivity of Ag-TiO_2/SiO_2

A two-variable Doehlert design (Table 1) was used to optimize the photodegradation of ACT on Ag-doped TiO_2/SiO_2 catalyst, in relation to working solution pH and temperature. Adsorption-desorption experiments were carried out for all the conditions of the Doehlert design and no appreciable ACT removal was observed during the 180-min runs (Supplementary Information, Fig. S2).

ACT concentrations over time fitted well to pseudo first-order (PFO) degradation models, with determination coefficients $R^2 > 0.96$ (Table 1). The highest ACT removal was 44.5%, corresponding to the calculated specific PFO degradation rate (k) of 4.77×10^{-3} min^{-1}, achieved for pH_0 8 and reaction temperature of 50 °C. Conversely, the lowest removal was 15.0%, with specific PFO degradation rate of 1.45×10^{-3} min^{-1} (pH 2 and 30 °C).

The response surface and contour plot (Fig. 7a-d) show that ACT % removal and specific degradation rate are higher with an increase in the initial pH of the medium. In fact, heterogeneous photocatalysis is strongly affected by the pH of the solution, due to the formation of oxidative radicals (Yang et al. 2008) and to the state of protonation of the contaminant and the semiconductor (Boukhatem

et al. 2017; Negarestani et al. 2020). The formation of $HO^{\bullet}$ radicals is enhanced at higher pH values, since more hydroxide ions are available on the catalyst surface and therefore, can be readily oxidized to form more hydroxyl radicals; which consequently improves ACT degradation (Galindo et al. 2000; Yang et al. 2008). Furthermore, the zero charge points of the main catalyst constituents, SiO_2 (pH_{ZPC} = 3.5) and TiO_2 (pH_{ZPC} = 6.3) imply that the catalyst surface is positively charged under acidic conditions ($pH < pH_{ZPC}$) and negatively charged in alkaline medium ($pH > pH_{ZPC}$) (Xu et al. 2006; Chiou et al. 2008; Yang et al. 2008). In addition, since the pKa of ACT is 9.5, it is positively charged in most of the pH range studied, which means that the electrostatic repulsion between the ACT molecules and the catalyst is increased at low pH (pH < 3.5) and also under highly alkaline conditions (pH > 9.5) (Yang et al. 2008; Negarestani et al. 2020). It is expected that ACT adsorption is decreased under these circumstances (pH < 3.5 and pH > 9.5), albeit no significant adsorption was observed in the adsorption-desorption experiments (Choina et al. 2013).

The effect of the temperature on ACT degradation is not so evident compared to that of pH. It was observed that the ACT degradation is slightly enhanced as temperature increases, especially when combined with high pH values. Considering that adsorption is not the main phenomenon in these reactions, it may be suggested that the improved efficiency is related to the greater amount of hydroxyl radicals formed on the catalyst surface. The ionic product of water (OH^-, H_3O^+ anions) increases as temperature rises, being correlated to the increase in the concentration of hydroxide ions. Once on the catalyst surface, these ions could quickly react with the positively charged holes generating a higher amount of $HO^{\bullet}$ radicals that can oxidize ACT, enhancing the photodegradation efficiency (Janus et al. 2012).

The Pareto chart (F-test with $p < 0.005$), illustrated in Fig. 7E, indicates that the independent variables (X_1 and X_2) and the quadratic terms (X_1^2 and X_2^2) of the polynomial model, corresponding to the pH and temperature variables, have statistically significant effects on the response (ACT % degradation). However, the Pareto chart (F-test with $p < 0.005$) for the degradation rate (Fig. 7F) shows that only the independent variable X_1 and the quadratic term X_2^2, corresponding to the linear effect of pH and to the quadratic effect of temperature, are statistically significant.

The corresponding quadratic response surface models that predict ACT % degradation and specific degradation rate as a function of the initial pH and solution temperature are given by Eqs. 2 (R^2 = 0.90) and 3 (R^2 = 0.88), respectively:

$$ACT\ degradation\ (\%) = 31.38 + 9.21X_1 + 5.74X_2 - 4.12{X_1}^2 + 9.87{X_2}^2 + 0.53X_1X_2 \quad (2)$$

$$k(min^{-1}) = 3.21 \times 10^{-3} + 1.12 \times 10^{-3}X_1 + 5.40 \times 10^{-4}X_2 - 2.70 \times 10^{-4}{X_1}^2 + 1.13 \times 10^{-3}{X_2}^2 - 1.50 \times 10^{-5}X_1X_2 \quad (3)$$

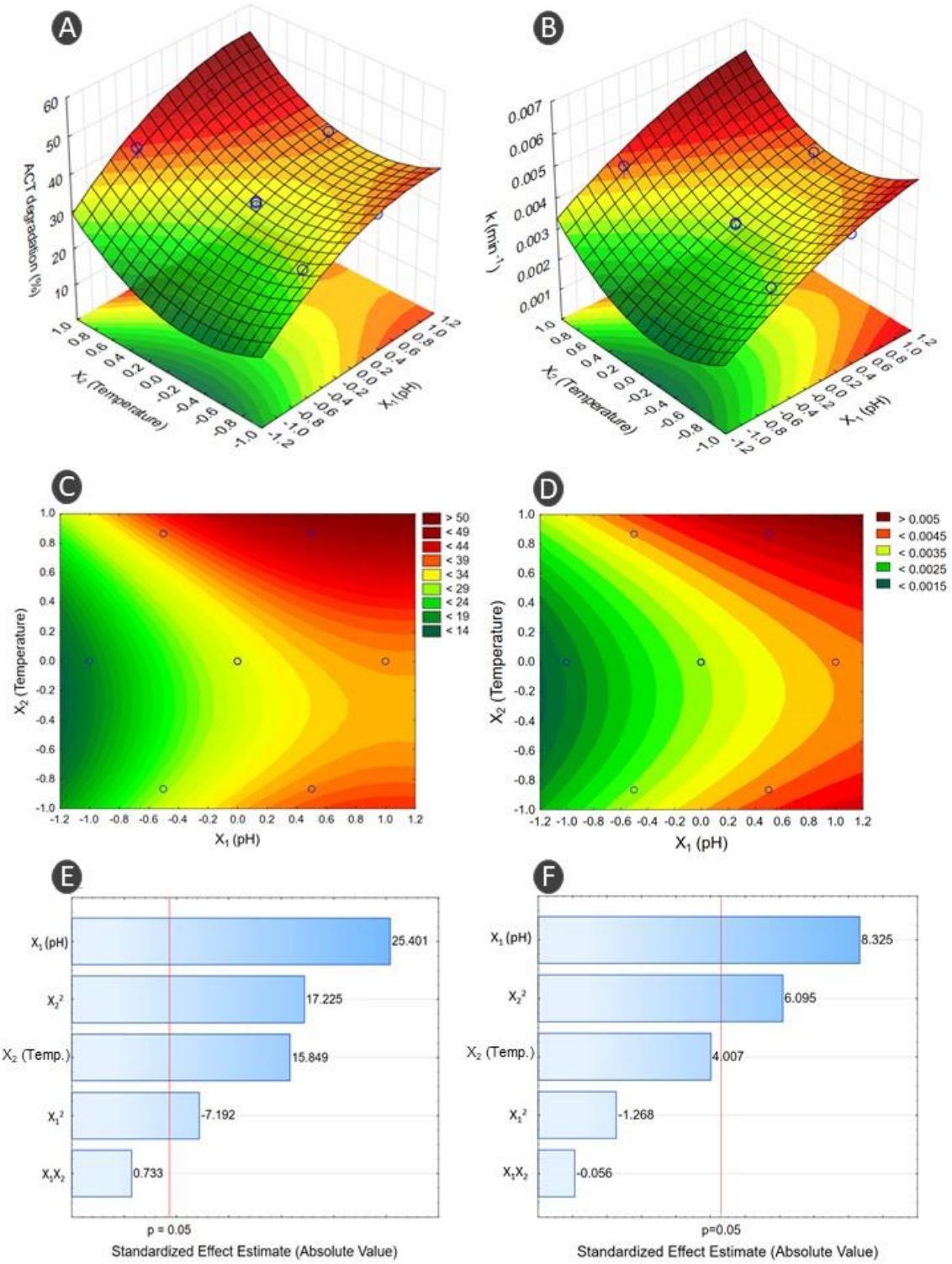

Fig. 7 a) and b) Response surfaces; c) and d) Contour plots; e) and f) Pareto charts for ACT % degradation and specific degradation rate (*k*). Conditions: 100 mg of Ag-TiO_2/SiO_2, 50 mL of 5-mg L^{-1} ACT solution, LED@430nm, pH varying in the range 2-10 (coded variable X_1 from –0.5 to 0.5) and temperature from 10 to 50 °C (coded variable X_2 from –0.866 to 0.866)

3.5. Investigation of reactive species

Different reactive species are generated during photocatalytic processes. In this context, various scavengers were used to quench specific species and evaluate their role in ACT degradation, according to Table 4 (Hernández-Uresti et al. 2016; Fan et al. 2018). The Ag-doped TiO_2/SiO_2 catalyst was used in the experiments and the conditions were chosen according to the Doehlert design. Central point conditions (run 4: pH_0 6; T = 30 °C) were adopted due to the significant ACT degradation achieved (31.4 ± 0.6%), combined to the fact that the ACT solution is already in the pH value required and the temperature is easy to control. Visible LEDs were used as the irradiation source.

Table 4 Scavengers used in the investigation of reactive species in ACT degradation over 120 min. Conditions: 100 mg of Ag-doped TiO_2/SiO_2, 50 mL of 5-mg L^{-1} ACT solution, LED@430nm, pH_0 6, T = 30 °C.

Scavenger[a]	Species quenched	Scavenger dosage (mol L^{-1})	ACT degradation (%)
Benzoquinone	Superoxide anion radicals ($O_2^{\bullet-}$)	0.02	2.9
Methanol	Hydroxyl radicals ($HO^{\bullet}$)	0.20	27.1
Potassium iodide	Holes (h^+)	0.02	92.1
No scavenger	-	-	31.4

[a]The concentrations of benzoquinone, KI and methanol were chosen based on Hernández-Uresti et al. (2016).

Among all the scavengers used in this work, benzoquinone led to the greatest suppression in the photocatalytic degradation of ACT (more than tenfold decrease), compared to the assay with no scavenger, in which 31.4% of ACT was degraded after 120 min. This result indicates that $O_2^{\bullet-}$ radical anions are the preeminent reactive species during ACT photodegradation on the Ag-doped TiO_2/SiO_2 catalyst. Nevertheless, it is important to mention that the semiquinone radicals ($Q^{\bullet-}$) formed in the reaction of benzoquinone with $O_2^{\bullet-}$ (Eq. 4) may subsequently react with $HO^{\bullet}$ (Eq. 5). This means that

$HO^{\bullet}$ radicals could be also quenched by the addition of benzoquinone, contributing to the decrease in the photodegradation efficiency (Schneider et al. 2020).

$$O_2^{\bullet -} + benzoquinone \rightarrow O_2 + Q^{\bullet -} \quad (4)$$

$$HO^{\bullet} + Q^{\bullet -} + H^+ \rightarrow H_2O + benzoquinone \quad (5)$$

When methanol was added to the system, ACT photodegradation was slightly suppressed (from 31.4% to 27.1%), implying that $HO^{\bullet}$ radicals are present in the reaction, but do not play as important a role as the superoxide radical anions. Nonetheless, the addition of potassium iodide to the reaction highly enhanced ACT photodegradation (an almost threefold increase), a result also found by Peng et al. (2017).. The authors suggest that this degradation boost could be due to the long life-time and high reactivity of the radicals formed through the reaction of I^- with h^+ or surface-bound $HO^{\bullet}$, with ACT molecules (Peng et al. 2017). Moreover, by quenching surface-bound h^+, KI could have hindered the h^+ and e^- recombination, and hence, contributed to the generation of other reactive species. In this situation, more electrons may be available to react with O_2 (Eq. 6), resulting in further $O_2^{\bullet -}$ radicals, which were already found to be the main reactive species during ACT photodegradation in our work (Low et al. 2017).

$$O_2 + e^- \rightarrow O_2^{\bullet -} \quad (6)$$

3.6. Effect of the initial concentration of ACT

The evaluation of the effect of the initial concentration of acetaminophen on its photodegradation kinetics was assessed by applying the Langmuir-Hinshelwood kinetic model (L-H). The experiments were performed with the Ag-doped TiO_2/SiO_2 catalyst, at pH_0 6 and temperature controlled at 30 °C (central point conditions; chosen according to the same reason described in section 3.5). Visible LEDs were used as the irradiation source.

From Fig. 8a, it can be seen that there is no significant difference in ACT degradation when 1 mg L^{-1} or 5 mg L^{-1} as initial concentration was used. However, when the initial concentration is increased from 10 mg L^{-1} to 50 mg L^{-1}, the degradation efficiency is sharply decreased. As remarked by Dimitrakopoulou et al. (2012), the rate of formation of active oxidizing species in the photocatalytic reaction depends on the amount of catalyst and photon flux. Keeping these conditions constant, it is expected that as the initial

concentration of the contaminant increases, the probability of the oxidizing radicals attacking the target molecules will also increase, thus increasing the degradation rate. However, at higher concentrations, the hydroxyl radicals formed are not sufficient for the amount of ACT molecules, leading to a reduction in the reaction rate and, consequently, to the transition of the apparent degradation kinetics from first to zero order. Therefore, it is expected that the rate of degradation will be lower at higher initial concentrations of ACT, since under these conditions, a greater amount of $HO^{\bullet}$ and $O_2^{\bullet-}$ radicals is needed to oxidize the ACT molecules. Moreover, the by-products formed in the reaction may absorb onto the active sites, leading to irreversible adsorption and consequently, to the photocatalyst deactivation, which is more evident for ACT initial concentrations greater than 10 mg L^{-1} (Gotostos et al. 2014).

The L-H model can be applied according to Eq. 7, where k_{int} (mg L^{-1} min^{-1}) corresponds to the intrinsic reaction rate constant, k (min^{-1}) is the PFO specific degradation rate and K_{ACT} (L mg^{-1}) is the contaminant adsorption constant onto the catalyst surface in the aqueous suspension (Chiou et al. 2008; Kumar et al. 2008). Fig. 8b shows that the degradation data for the Ag-doped TiO_2/SiO_2 was successfully fitted to the L-H model. A satisfactory linear correlation was achieved (R^2 = 0.90), with k_{int} = 2.71 × 10^{-4} mmol L^{-1} min^{-1} and K_{ACT} = 11.11 L $mmol^{-1}$. Gotostos et al. 2014 found results in the same order of magnitude, by photodegrading ACT using a $K_3[Fe(CN)_6]/TiO_2$ catalyst, achieving k_{int} = 6.54 × 10^{-4} mmol L^{-1} min^{-1} and K_{ACT} = 17.27 L $mmol^{-1}$.

$$\frac{1}{k} = \frac{1}{k_{int}}[ACT]_0 + \frac{1}{k_{int}\,K_{ACT}} \quad (7)$$

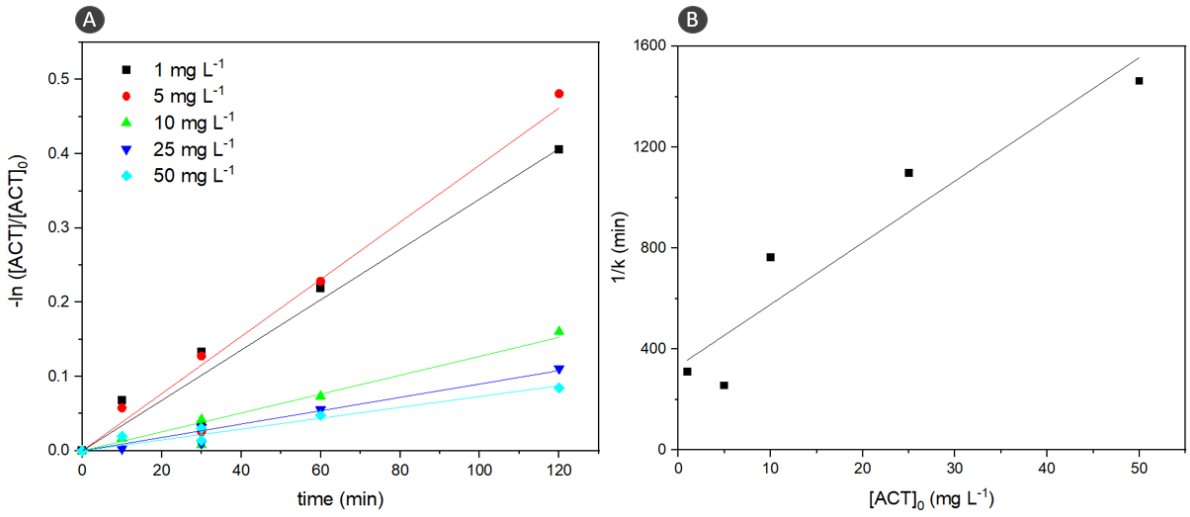

Fig. 8 a) Pseudo first-order ACT degradation at different initial concentrations; b) Linearized Langmuir-Hinshelwood (L-H) kinetics. Conditions: 100 mg of Ag-TiO_2/SiO_2, 50 mL of ACT solution at different concentration, LED@430nm, pH_0 6, T = 30 °C.

4. Conclusions

The Ag-doped TiO_2/SiO_2 catalyst showed the best photocatalytic activity under visible light in acetaminophen (ACT) degradation ($k = 4.0 \times 10^{-3}$ min^{-1}) in a batch system. The undoped sample did not show any activity under visible light. The TiO_2 crystal size was smaller in the doped catalysts compared to pure TiO_2/SiO_2. EDS analysis identified the doping elements in the catalyst structures, and SEM images showed that the TiO_2 nanocrystals were satisfactorily supported on the silica gel surface. In ACT photodegradation under UV light, the ZnO@S-doped catalyst showed the best performance, reaching $k = 8.1 \times 10^{-3}$ min^{-1}. Using a suitable response-surface investigation, we concluded that the optimum reaction conditions for the Ag-TiO_2/SiO_2 catalyst were, respectively, pH_0 8 and T = 50 °C. Both variables were shown to be statistically significant, being the pH even more determinant for the catalyst performance. With regard to the catalyst stability over successive reuse cycles, we showed that visible-light activity was reduced due to TiO_2 leaching from the support surface. However, after the reuse under UV irradiation, the catalyst activity improved, and more intense peaks were observed in the EDS referring to Ag^0, suggesting that Ag^+ ions were photo-reduced to Ag^0 by UV light, acting as a co-catalyst and boosting the efficiency of the photocatalytic ACT degradation. Experiments were performed with radical scavengers to elucidate the main reactive pathway, and we concluded that the superoxide radical anion was the most active species in the photodegradation of the model pollutant using the Ag-TiO_2/SiO_2 catalyst. Finally, the Langmuir-Hinshelwood (L-H) kinetic expression was satisfactorily applied for ACT degradation using the Ag-doped TiO_2/SiO_2 catalyst, with k_{int} = 0.041 mg L^{-1} min^{-1} and K_{ACT} = 0.074 L mg^{-1}. In conclusion, it was shown that the doping of TiO_2 catalysts supported on silica gel is a promising alternative in technologies for the removal of pharmaceuticals from aqueous effluents.

Acknowledgements

This study was financed in part by the Coordenação de Aperfeiçoamento de Pessoal de Nível Superior – Brasil (CAPES) – Finance Code 001. The authors also express their gratitude to the National

Council of Scientific and Technological Development (CNPq, Brazil), and to the São Paulo Research Foundation (FAPESP, grants # 2016/00953-6 and # 2018/21271-6) for the financial support.

Declarations

• Ethics approval and consent to participate

Not applicable.

• Consent for publication

Not applicable.

• Availability of data and materials

All data generated or analyzed during this study are included in this published article and its supplementary information file.

• Competing interests

The authors declare that they have no competing interests.

• Funding

Coordenação de Aperfeiçoamento de Pessoal de Nível Superior - Brasil (CAPES - Coordination for the Improvement of Higher Education Personnel) – Finance Code 001, National Council for Scientific and Technological Development (CNPq) and the São Paulo Research Foundation (FAPESP, grant #2018/21271-6).

• Authors' contributions

CAG: Conceptualization, Methodology, Validation, Formal analysis, Investigation, Writing - Original Draft, Visualization.

PHP: Methodology, Validation, Formal analysis, Investigation, Writing - Original Draft, Visualization.

BR: Formal analysis, Investigation, Writing – Original Draft, Visualization.

ACSCT: Conceptualization, Validation, Resources, Writing - Original Draft, Writing - Review & Editing, Supervision, Funding acquisition.

All authors read and approved the final manuscript.

REFERENCES

Aini, N., Rachman, S., Maunatin, A., Syarifah, A. (2019) Synthesis, characterization and antibacterial

activity of silver doped TiO_2 photocatalyst. AIP Conference Proceedings 2120:0500171-0500176.

Akpotu SO, Oseghe EO, Ayanda OS, et al (2019) Photocatalysis and biodegradation of pharmaceuticals in wastewater: effect of abiotic and biotic factors. Clean Technol Environ Policy 21:1701–1721.

Alhaji MH, Sanaullah K, Khan A, et al (2017) Recent developments in immobilizing titanium dioxide on supports for degradation of organic pollutants in wastewater- A review. Int J Environ Sci Technol 14:2039–2052.

Bischoff BL, Anderson MA (1995) Peptization Process in the Sol-Gel Preparation of Porous Anatase (TiO_2). Chem Mater 70:1772–1778

Boukhatem H, Khalaf H, Djouadi L, et al (2017) Diclofenac degradation using mont-La (6%)-Cu^0.6Cd^0.4S as photocatalyst under NUV-Vis irradiation. Operational parameters, kinetics and mechanism. J Environ Chem Eng 5:5636–5644.

Boyjoo Y, Sun H, Liu J, et al (2017) A review on photocatalysis for air treatment: From catalyst development to reactor design. Chem. Eng. J. 310:537–559

Carp O, Huisman CL, Reller A (2004) Photoinduced reactivity of titanium dioxide. Prog Solid State Chem 32:33–177.

Chen D, Cheng Y, Zhou N, et al (2020) Photocatalytic degradation of organic pollutants using TiO_2-based photocatalysts: A review. J Clean Prod 268:121725.

Chen X, Sun H, Zhang J, et al (2019) Cationic S-doped TiO_2/SiO_2 visible-light photocatalyst synthesized by co-hydrolysis method and its application for organic degradation. J Mol Liq 273:50–57.

Chen Y, Wang K, Lou L (2004) Photodegradation of dye pollutants on silica gel supported TiO_2 particles under visible light irradiation. J Photochem Photobiol A Chem 163:281–287.

Chiou CH, Wu CY, Juang RS (2008) Influence of operating parameters on photocatalytic degradation of phenol in UV/TiO2 process. Chem Eng J 139:322–329.

Choi W, Termin A, Hoffmann MR (1994) The role of metal ion dopants in quantum-sized TiO_2: Correlation between photoreactivity and charge carrier recombination dynamics. J Phys Chem 98:13669–13679.

Choina J, Kosslick H, Fischer C, et al (2013) Photocatalytic decomposition of pharmaceutical ibuprofen pollutions in water over titania catalyst. Appl Catal B Environ 129:589–598.

Chu H, Lin YH, Lin CY (2017) Characterization, degradation, and reaction pathways of indoor toluene over visible-light-driven S, Zn Co-doped TiO_2. IOP Conf Ser Earth Environ Sci 51:102001.

Dey D, Halder N, Misra KP, et al (2020) Systematic study on the effect of Ag doping in shaping the magnetic properties of sol-gel derived TiO_2 nanoparticles. Ceram Int 46:27832–27848.

Dimitrakopoulou, Despina, et al. (2012) Degradation, mineralization and antibiotic inactivation of amoxicillin by UV-A/TiO_2 photocatalysis. J Environ Manage 98:168−174.

Doehlert DH (1970) Uniform Shell Designs. Appl Stat 19:231–239.

Fan G, Peng H, Zhang J, et al (2018) Degradation of acetaminophen in aqueous solution under visible light irradiation by Bi-modified titanate nanomaterials: Morphology effect, kinetics and mechanism. Catal Sci Technol 8:5906–5919.

Gadipelly C, Pérez-González A, Yadav GD, et al (2014) Pharmaceutical industry wastewater: Review of the technologies for water treatment and reuse. Ind Eng Chem Res 53:11571–11592.

Galindo C, Jacques P, Kalt A (2000) Photodegradation of the aminoazobenzene acid orange 52 by three advanced oxidation processes: UV/H_2O_2, UV/TiO_2 and VIS/TiO_2. J Photochem Photobiol A Chem 130:35–47.

Gotostos MJN, Su CC, De Luna MDG, Lu MC (2014) Kinetic study of acetaminophen degradation by visible light photocatalysis. J Environ Sci Heal - Part A Toxic/Hazardous Subst Environ Eng 49:892–899.

Hashimoto K, Irie H, Fujishima A (2006) TiO_2 Photocatalysis: A historical overview and future prospects. Jpn J Appl Phys 44:8269–8285

Hernández-Uresti DB, Vázquez A, Sanchez-Martinez D, Obregón S (2016) Performance of the polymeric g-C_3N_4 photocatalyst through the degradation of pharmaceutical pollutants under UV-vis irradiation. J Photochem Photobiol A Chem 324:47–52.

Ibrahim NS, Leaw WL, Mohamad D, et al (2020) A critical review of metal-doped TiO_2 and its structure-physical properties-photocatalytic activity relationship in hydrogen production. Int J Hydrogen Energy 45:28553–28565.

Ikehata K, Jodeiri Naghashkar N, Gamal El-Din M (2006) Degradation of aqueous pharmaceuticals by ozonation and advanced oxidation processes: A review. Ozone Sci Eng 28:353–414.

Janus M, Kusiak-Nejman E, Morawski AW (2012) Influence of water temperature on the photocatalytic activity of titanium dioxide. React Kinet Mech Catal 106:289–295.

Kanakaraju D, Glass BD, Oelgemöller M (2014) Titanium dioxide photocatalysis for pharmaceutical wastewater treatment. Environ Chem Lett 12:27–47.

Kanakaraju D, Glass BD, Oelgemöller M (2018) Advanced oxidation process-mediated removal of pharmaceuticals from water: A review. J Environ Manage 219:189–207.

Kim W, Tachikawa T, Kim H, et al (2014) Visible light photocatalytic activities of nitrogen and platinum-doped TiO_2: Synergistic effects of co-dopants. Appl Catal B Environ 147:642–650.

Kumar KV, Porkodi K, Rocha F (2008) Langmuir-Hinshelwood kinetics - A theoretical study. Catal Commun 9:82–84.

Lim TH, Kim SD (2004) Trichloroethylene degradation by photocatalysis in annular flow and annulus fluidized bed photoreactors. Chemosphere 54:305–312.

Low J, Jiang C, Cheng B, et al (2017) A Review of Direct Z-Scheme Photocatalysts. Small methods 1700080:1–21.

Martignac M, Oliveros E, Maurette MT, Claparols C, Benoit-Marquié F (2013) Mechanistic pathways of the photolysis of paracetamol in aqueous solution: An example of photo-Fries rearrangement. Photochem. Photobiol. Sci. 12:527−535.

Mazabuel-Collazos A, Rodríguez-Páez JE (2018) Chemical Synthesis and Characterization of ZnO-TiO_2 semiconductor nanocomposites: Tentative mechanism of particle formation. J Inorg Organomet Polym Mater 28:1739–1752.

Mohapatra DP, Brar SK, Tyagi RD, et al (2014) Analysis and advanced oxidation treatment of a persistent pharmaceutical compound in wastewater and wastewater sludge-carbamazepine. Sci Total Environ 470–471:58–75.

Murgolo S, De Ceglie C, Di Iaconi C, Mascolo G (2021) Novel TiO_2-based catalysts employed in photocatalysis and photoelectrocatalysis for effective degradation of pharmaceuticals (PhACs) in water: A short review. Curr Opin Green Sustain Chem 30:100473.

Negarestani M, Motamedi M, Kashtiaray A, et al (2020) Simultaneous removal of acetaminophen and ibuprofen from underground water by an electrocoagulation unit: Operational parameters and kinetics. Groundw Sustain Dev 11:100474.

Nguyen LT, Nguyen HT, Pham TD, et al (2020) UV-visible light driven photocatalytic degradation of ciprofloxacin by N,S Co-doped TiO_2: The effect of operational parameters. Top Catal 63:985–995.

Niu Y, Xing M, Tian B, Zhang J (2012) Improving the visible light photocatalytic activity of nano-sized titanium dioxide via the synergistic effects between sulfur doping and sulfation. Appl Catal B Environ 115–116:253–260.

Ohno T, Akiyoshi M, Umebayashi T, et al (2004) Preparation of S-doped TiO_2 photocatalysts and their photocatalytic activities under visible light. Appl Catal A Gen 265:115–121.

Paumo HK, Dalhatou S, Katata-Seru LM, et al (2021) TiO_2 assisted photocatalysts for degradation of emerging organic pollutants in water and wastewater. J Mol Liq 331:115458.

Peng H, Chen Y, Mao L, Zhang X (2017) Significant changes in the photo-reactivity of TiO_2 in the presence of a capped natural dissolved organic matter layer. Water Res 110:233–240.

Ramos B, Carneiro JG de M, Nagamati LI, Teixeira ACSC (2021) Development of intensified flat-plate packed-bed solar reactors for heterogeneous photocatalysis. Environ Sci Pollut Res. 28: 24023–24033.

Rincón GJ, La Motta EJ (2019) A fluidized-bed reactor for the photocatalytic mineralization of phenol on TiO_2-coated silica gel. Heliyon 5:e01966.

Rivera-Utrilla J, Sánchez-Polo M, Ferro-García MÁ, et al (2013) Pharmaceuticals as emerging contaminants and their removal from water. A review. Chemosphere 93:1268–1287.

Rogowska J, Cieszynska-Semenowicz M, Ratajczyk W, Wolska L (2020) Micropollutants in treated wastewater. Ambio 49:487–503.

Schneider JT, Firak DS, Ribeiro RR, Peralta-Zamora P (2020) Use of scavenger agents in heterogeneous photocatalysis: truths, half-truths, and misinterpretations. Phys Chem Chem Phys 22:15723–15733.

Taoufik N, Boumya W, Achak M, et al (2021) Comparative overview of advanced oxidation processes and biological approaches for the removal pharmaceuticals. J Environ Manage 288:112404.

Tobajas M, Belver C, Rodriguez JJ (2017) Degradation of emerging pollutants in water under solar irradiation using novel TiO_2.ZnO/clay nanoarchitectures. Chem Eng J 309:596–606.

Wei F, Ni L, Cui P (2008) Preparation and characterization of N-S-codoped TiO_2 photocatalyst and its photocatalytic activity. J Hazard Mater 156:135–140.

Xu M, Wang Y, Geng J, Jing D (2017) Photodecomposition of NOx on Ag/TiO_2 composite catalysts in a gas phase reactor. Chem Eng J 307:181–188.

Xu P, Wang H, Tong R, et al (2006) Preparation and morphology of SiO_2/PMMA nanohybrids by microemulsion polymerization. Colloid Polym Sci 284:755–762.

Yang L, Yu LE, Ray MB (2008) Degradation of paracetamol in aqueous solutions by TiO_2 photocatalysis. Water Res 42:3480–3488.

Zhang H, Jiang Y, Zhou B, et al (2021) Preparation and photocatalytic performance of silver-modified

and nitrogen-doped TiO_2 nanomaterials with oxygen vacancies. New J Chem 45:4694–4704.

Zhou K, Ding Y, Zhang L, et al (2020) Synthesis of mesoporous ZnO/TiO_2-SiO_2 composite material and its application in photocatalytic adsorption desulfurization without the addition of an extra oxidant. Dalt Trans 49:1600–1612.

Zielińska-Jurek A, Zaleska A (2014) Ag/Pt-modified TiO_2 nanoparticles for toluene photooxidation in the gas phase. Catal Today 230:104–111.